Thermal relaxation of supercritical fluids by equilibrium molecular dynamics

Huaqiang Luo and Giovanni Ciccotti
Centre Européen de Calcul Atomique et Moléculaire, Ecole Normale Supérieure de Lyon, allée d'Italie 46, 69364 Lyon Cedex 7, France

Michel Mareschal
Université Libre de Bruxelles, Faculté des Sciences, Case Postale 231, B1050 Bruxelles, Belgique

Madeleine Meyer*
Laboratoire des Solides Irradiés, CNRS URA 1380, CEA/DTA/CEREM/DECM, École Polytechnique, F91128 Palaiseau Cedex, France

Bernard Zappoli
Centre National d'Études Spatiales, 18 Avenue E. Belin, 31055 Toulouse Cedex, France
(Received 18 July 1994)

Two-dimensional molecular dynamics (MD) simulations are performed in the NVT ensemble (constant number of particles, volume, and temperature) with a truncated and shifted Lennard-Jones potential in order to model highly compressible fluids near the critical point. The thermodynamic and transport properties are computed for three different supercritical states (same critical density and different temperatures) and one "normal" fluid with a different density. The static properties are obtained from the relevant equilibrium fluctuations while the time-dependent properties are computed here in terms of the equilibrium time-correlation functions (TCF's). The TCF's of local density, current, as well as temperature are calculated. The thermal diffusivity and the sound velocity decrease when the temperature is approaching the critical temperature, thus showing the expected behavior. However, this behavior is only a nearly critical one, since this study has been performed in a temperature range where the hydrodynamic description still appears to be valid. Indeed, good agreement has been found between the equilibrium fluctuations computed by MD and hydrodynamics. The time scales for the normal and the supercritical fluids are quite different: a considerably slower decay of the fluctuation relaxations is observed in supercritical fluids.

PACS number(s): 05.60.+w, 05.70.−a, 05.40.+j, 64.60.Fr

I. INTRODUCTION

The study of the hydrodynamic behavior of supercritical pure fluids has fundamental as well as applied motivations. The fundamental interest lies in the unusual heat and mass transport near the critical point, which is due to the divergence of the compressibility and the vanishing of the heat diffusivity. The transport mechanisms are dominated by acoustic phenomena as has been shown both by numerical and asymptotic analyses of one-dimensional Navier-Stokes equations applied to a van der Waals fluid [1–3]. Heat transport is strongly enhanced by thermoacoustic couplings, so that heat propagation is much faster than it would be, if only diffusion contributed to it. The experiments, which allow us to study these phenomena, can only be performed under the microgravity conditions that prevail in spacecrafts [4–6]; indeed, on ground, the presence of strong convective instabilities or density stratifications would hide the transport phenomenon itself. On the other hand, the study of critical transport is also linked to space applications since the fluid (and fuel) storage in the microgravity conditions of space flights is usually at temperatures above critical.

The proximity of the critical point [7] is expressed by the fluid through different effects: First, while approaching the critical point located at number density $n=n_c$ and temperature $T=T_c$, the compressibility of the fluid becomes large (as a matter of fact, much larger than that of a perfect gas) and several thermodynamic properties have unusual values leading, in turn, to a behavior that, although uncommon, is still consistent with hydrodynamic theory [8]. Very near the critical point, other phenomena might occur that are linked to the divergence of the correlation length ξ, becoming much larger than any wavelength; in this region the hydrodynamic description itself becomes inadequate [9].

In this paper, we will focus on the study of fluid properties in the first region: By a supercritical fluid, we understand, in the remainder of the article, a highly compressible fluid still obeying the Navier-Stokes hydrodynamic equations. Our aim will be to investigate, at a microscopic scale, the supercritical fluid behavior. In order to do so, we will first limit ourselves to the study of the equilibrium fluctuations. The dynamic structure factor, for instance, has already been studied by the molecular dynamics (MD) technique [10] in different atomic models, showing the validity of the hydrodynamic description up to the atomic scale [11]. We will, in the

*Author to whom correspondence should be addressed.

present study, extend the technique to the proximity of the critical point in order to investigate and probe the fluid behavior. Our rationale will be to compare the MD-computed fluctuation spectrum with the one generated from hydrodynamics, given the values of the transport coefficients.

The difficulty of performing simulations of fluid behavior near a critical point arises both from large fluctuations and slow relaxations. Thus simulations require large system sizes and long-time trajectories. However, significant results have already been obtained for static equilibrium properties; in particular, the liquid-gas coexistence curve has been computed for the Lennard-Jones model [12–14]. Another study also performed in the two-phase region concerns the temperature dependence of the liquid-vapor interface simulated with a two-dimensional (2D) Lennard-Jones model [15]. It is worth noting that the finite size of the systems used in the molecular dynamics and Monte Carlo (MC) simulations results in the fact that the critical point is not well defined, but, nevertheless, characteristic features of the critical behavior are obtained [14,16]. In particular, MC results clearly show the existence of strong density fluctuations with relatively large length scales. Moreover, a large value of the isothermal compressibility is obtained near the estimated critical temperature. It is, however, not easy to obtain an accurate value of the compressibility derived from the density fluctuations, since this method of evaluation is strongly size dependent [14].

In this work, the model used to represent a highly compressible fluid is a two-dimensional system that contains particles interacting via a Lennard-Jones potential. The specific heats, the isothermal compressibility, as well as the speed of sound, are determined by an ensemble average of the relevant thermal fluctuations generated by MD. The time-dependent properties are investigated here in terms of the equilibrium time-correlation functions (TCF's) that, according to the linear response theory, contain the full information on the near-equilibrium relaxation. The TCF's of the local density, the current, as well as the temperature, are calculated. The self-diffusion coefficient, the thermal conductivity, and the bulk and shear viscosity are also computed [17].

Very near the critical point, the large density fluctuations and the correlation length reaching the order of magnitude of the system would induce unrealistically heavy computations. In this region the hydrodynamic description would also be questionable. We have therefore restricted ourselves to states sufficiently far from T_c so that sensible averages can be performed. The agreement between the two descriptions, MD and linearized Navier-Stokes, shows indeed the validity of the hydrodynamic equations in the states reached by the simulation technique. In this sense, we are able to describe the effects of a high compressibility of the fluid on the dynamic properties (rather than get so close to the critical point that mode coupling effects would become important). In a second (forthcoming) paper, we will use the model to investigate the nonequilibrium behavior of a highly compressible fluid.

Simulations performed on a fluid far from (T_c, n_c), a "normal" fluid, will allow us to compare typical behaviors. For instance, the temperature fluctuation relaxation, which is usually dominated by the slow entropy diffusive mode, will, near (T_c and n_c), propagate according to the fast acoustic modes. We shall relate this behavior to the fast heat transport observed in experiments.

The outline of the paper is as follows. In Sec. II, we introduce the MD model system as well as the microscopic definitions of the thermodynamic quantities. The results of the MD calculations and those obtained from hydrodynamic theory are shown and discussed in Sec. III. Finally, in the conclusion, we relate the observed behavior to the experimental results and we comment on the perspectives offered by the microscopic approach.

II. METHOD

A. Model system

In the MD study, a two-dimensional fluid system of $N=256$ particles interacting with the Lennard-Jones (LJ) potential

$$u(r_{ij})=4\varepsilon\left[\left[\frac{\sigma}{r_{ij}}\right]^{12}-\left[\frac{\sigma}{r_{ij}}\right]^{6}\right] \tag{1}$$

is considered. To simplify the MD calculations, this potential is truncated and shifted with a cutoff radius of 2.5σ. This simple 2D model enables us to study relatively large wavelengths; to reach comparable values, a three-dimensional (3D) system would require more than 4000 particles. This 2D model also allows us to perform long-time trajectories that are, in general, needed to study hydrodynamic behavior, this is even more so near the critical point.

In this work, ε, σ and $\tau=\sqrt{m\sigma^2/48\varepsilon}$ are chosen as the energy, length, and time units, respectively. The temperature unit is ε/k_B; furthermore, the Boltzmann constant k_B is set to 1 and the atomic mass is chosen to be $m=48$. The time step in the MD runs is taken as 0.032, which corresponds to 0.01 ps for liquid argon ($\sigma=0.3405$ nm, $\varepsilon/k_B=119.8$ K). As explained hereafter we are primarily interested in the temperature dependence of the model system; therefore MD runs are performed in the NVT (constant number of particles, volume, and temperature) ensemble, where the temperature is fixed by the Nosé-Hoover thermostat [18].

The phase diagram of the truncated and shifted 2D-LJ model fluid has been studied in detail in previous works. The estimated value of the critical point is given by $T_c=0.46$ and $n_c=0.34$ [13]. In the present work, three supercritical states at critical density ($n_c=0.34$) are investigated. To avoid the extreme fluctuations at the critical point, we have performed the simulations in a temperature range located in the supercritical region. The lowest temperature investigated is $T=0.5$. The nearly critical behavior of the physical properties (e.g., the increase of the compressibility) will thus be characterized as a function of the temperature. Besides the three supercritical states, a normal fluid state has also been studied.

This enables us to compare the supercritical fluid with the better understood normal fluid. The location of the four states is shown in Fig. 1, where the phase diagram of the model fluid in the critical region is also displayed. The simulations made are usually 10^6 time steps long, except for state 4 where shorter trajectories of 250 000 time steps were already giving a comparable accuracy, this difference is due, of course, to the proximity of the critical point.

B. Thermodynamic properties from fluctuations

The equilibrium thermal fluctuations of energy, pressure, and density are computed by MD. The specific heat per particle at constant volume c_v, the isothermal compressibility κ_T, as well as $(\partial P/\partial T)_V$ for the model fluid are obtained from these fluctuations using the following relations [19]:

$$c_v=\frac{1}{k_B NT^2}[\langle(\hat{E})^2\rangle-\langle\hat{E}\rangle^2]_{\mathrm{NVT}}$$
$$=1+\frac{1}{k_B NT^2}[\langle(\hat{U})^2\rangle-\langle\hat{U}\rangle^2]_{\mathrm{NVT}}\ , \tag{2}$$

$$\kappa_T=-\frac{1}{V}\left[\frac{\partial V}{\partial P}\right]_T=\frac{V}{k_B NT}\lim_{k\to 0,t\to 0}F(k,t)\ , \tag{3}$$

$$\left[\frac{\partial P}{\partial T}\right]_V=\frac{1}{k_B T^2}\langle(\hat{U}-\langle\hat{U}\rangle)(\hat{P}-\langle\hat{P}\rangle)\rangle_{\mathrm{NVT}}+k_B n\ , \tag{4}$$

where $\hat{E}$ and $\hat{U}$ are the total and potential energy, respectively, $\hat{P}$ is the pressure, $F(k,t)$ is the number density TCF, which will be defined in Sec. II C, and the brackets $\langle\ \rangle$ indicate an ensemble average.

From the above quantities, the specific heat per particle at constant pressure c_p and the speed of sound c_s can be also obtained by using

$$c_p-c_v=-T\left[\frac{\partial P}{\partial T}\right]_V^2\left[\frac{\partial V}{\partial P}\right]_T=\frac{VT}{N}\left[\frac{\partial P}{\partial T}\right]_V^2\kappa_T\ , \tag{5}$$

$$c_s=\left[\frac{c_p}{c_v m}\left[\frac{\partial P}{\partial n}\right]_T\right]^{1/2}=\left[\frac{c_p}{c_v mn\kappa_T}\right]^{1/2}. \tag{6}$$

C. Dynamic properties in terms of TCF's

In the MD study, we consider the TCF's for the local density $F(k,t)$, the longitudinal current $V(k,t)$, and the local temperature $T(k,t)$. The first two TCF's can be calculated straightforwardly by

$$F(k,t)=\frac{1}{N}\left\langle\sum_{i=1}^{N}e^{i\mathbf{k}\cdot\mathbf{r}_i(0)}\sum_{j=1}^{N}e^{-i\mathbf{k}\cdot\mathbf{r}_j(t)}\right\rangle\ , \tag{7}$$

$$V(k,t)=\frac{\mathbf{k}}{N}\cdot\left\langle\sum_{i=1}^{N}\boldsymbol{\nu}_i e^{i\mathbf{k}\cdot\mathbf{r}_i(0)}\sum_{j=1}^{N}\boldsymbol{\nu}_j e^{-i\mathbf{k}\cdot\mathbf{r}_j(t)}\right\rangle\cdot\mathbf{k}\ . \tag{8}$$

There is no thermodynamic prescription that permits the microscopic definition of the local instantaneous temperature out of equilibrium [20]. Here, we use the temperature definition based on the local equilibrium assumption. The latter is implicitly defined by

$$\delta e=\left[\frac{\partial e}{\partial n}\right]_T\delta n+\left[\frac{\partial e}{\partial T}\right]_n\delta T\ , \tag{9}$$

where δ stands for fluctuation and e denotes the energy density. The partial derivatives are equilibrium derivatives. The microscopic definitions of the instantaneous local temperature fluctuations will be discussed in detail in a separate paper.

In k space $[f_k=(1/V)\int e^{-i\mathbf{k}\cdot\mathbf{r}}f(r)dr]$, Eq. (9) can be written as

$$Nc_v\hat{T}(k,t)=\sum_{i=1}^{N}\left[\frac{1}{2}\left[m\nu_i^2(t)+\sum_{j\neq i}^{N}\phi_{ij}(t)\right]-\left[\frac{\partial e}{\partial n}\right]_T\right]e^{-i\mathbf{k}\cdot\mathbf{r}_i(t)}\ , \tag{10}$$

where $(\partial e/\partial n)_T$ can be explicitly computed from

$$\left[\frac{\partial e}{\partial n}\right]_T=-\frac{1}{n}\left[\frac{\partial E}{\partial V}\right]_T+\frac{E}{N}=\frac{1}{n}\left\{-\left[T\left[\frac{\partial p}{\partial T}\right]_V-p\right]+e\right\}=-\frac{T}{n}\left[\left[\frac{\partial p}{\partial T}\right]_V+h\right]\ , \tag{10'}$$

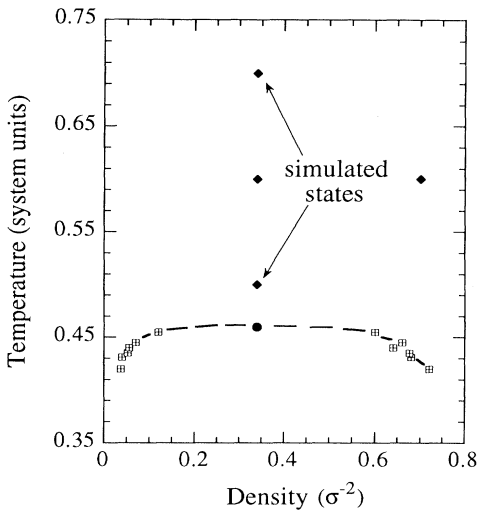

FIG. 1. Phase diagram of the truncated and shifted 2D Lennard-Jones fluid (from Smit [13]). The four states investigated in our simulations are indicated by the squares and the estimated value of the critical point [13] by a filled circle.

with h the enthalpy density.

Based on linearized Navier-Stokes hydrodynamic equations and equilibrium static fluctuations values, the hydrodynamic limit ($k \to 0$) of the TCF's is given by the so-called Landau-Placzek formula, which reads [21]

$$\frac{F(k,t)}{F(k,0)} = \frac{\gamma-1}{\gamma} e^{-D_r k^2 t} + \frac{1}{\gamma} e^{-\Gamma k^2 t}[\cos(c_s k t) + b(k)\sin(c_s k t)] , \tag{11}$$

$$\frac{V(k,t)}{V(k,0)} = \frac{e^{-\Gamma k^2 t}\{c_s k[\cos(c_s k t) + b(k)\sin(c_s k t)] - 2\Gamma k^2[\sin(c_s k t) - b(k)\cos(c_s k t)]\}}{c_s k + 2\Gamma k^2 b(k)} , \tag{12}$$

$$\frac{T(k,t)}{T(k,0)} = \frac{1}{\gamma} e^{-D_T k^2 t} + \left[\frac{\gamma-1}{\gamma}\right] e^{-\Gamma k^2 t}\left[\cos(c_s k t) + \frac{k}{c_s}[\Gamma - D_T(\gamma+1)]\sin(c_s k t)\right] , \tag{13}$$

with

$$\gamma = c_p / c_v , \tag{14}$$

$$D_T = \lambda / n c_p , \tag{15}$$

$$\Gamma = \tfrac{1}{2}[(\gamma-1)D_T + \eta/mn] , \tag{16}$$

$$b(k) = [\Gamma + D_T(\gamma-1)]k/c_s , \tag{17}$$

and

$$\frac{T(k,t)}{T(k,0)} = \frac{\langle \hat{T}(k,t)\hat{T}(-k,0)\rangle}{\langle \hat{T}(k,0)\hat{T}(-k,0)\rangle} . \tag{18}$$

The ratio of the specific heats γ, the thermal diffusivity D_T, the sound attenuation coefficient Γ, as well as the speed of sound c_s, can be evaluated either by fitting the theoretical solutions [Eqs. (11)–(13)] to the MD-generated TCF's, or by direct MD calculation. In this work, we have chosen the direct MD calculation. Indeed, as will be seen in the following, a reasonable agreement is obtained between the TCF's calculated by MD and those predicted by the hydrodynamic theory using the independently determined parameters. The thermal conductivity λ and the viscosity $\eta = \eta_s + \zeta$, η_s being the shear viscosity and ζ the bulk viscosity, are calculated with the well-known Green-Kubo formulas [22]. The heat capacities c_P and c_v are computed by MD using relations (2), (3), and (5); then the values of γ, D_T, and Γ are obtained with relations (14)–(16).

III. RESULTS AND DISCUSSION

A. Thermodynamics of the simulated states

The thermodynamic properties of the four states investigated by MD with the 2D LJ model are listed in Table I. The density and temperature allow one to locate the states in Fig. 1. The system size selected for almost all the computations corresponds to $N = 256$. The pressure P and the potential energy U have been computed together with the self-diffusion coefficient D. The results are obtained with the truncated and shifted potential without any long-range corrections.

The standard deviation of the density Δn given in Table I is calculated locally with the block density distribution technique (see Ref. [14]). For this purpose, the 2D system is divided into 4×4 subsystems where the number of particles are recorded and analyzed. As expected for computations performed at the critical density (states 1–3), the pressure increases with the temperature whereas the energy decreases. The self-diffusion coefficient D is calculated by integrating the velocity-autocorrelation (VAC) function using the Green-Kubo formula [22],

$$D = \tfrac{1}{2}\int_0^{n_\tau} dt \langle \boldsymbol{v}_i(t)\cdot\boldsymbol{v}_i(0)\rangle . \tag{19}$$

The VAC is integrated in a time range $n_\tau = 100\tau$ for the supercritical states and $n_\tau = 25\tau$ for the normal fluid. The integration is limited here by the acoustic recurrence time τ_s (see Table III) as will be discussed later. However, the VAC's decay to almost, though not exactly, zero within the integrated time, as shown in Fig. 2. The values obtained for D at critical density are comparable to the Enskog values for hard disks at the same density and temperatures. There does not seem to be any peculiarity in the values for the diffusion coefficient, although the time scale over which the velocity correlations remain noticeable is much larger than in liquids. The same holds for the heat conductivity Green-Kubo integrand, which is also displayed in Fig. 2; although it remains different from zero for a relatively long time, this can be accounted for by the low critical density. The time dependence seems otherwise similar to the liquid behavior, in particu-

TABLE I. Thermodynamic properties of the simulated states.

State	$T(\varepsilon/k_B)$	$n(\sigma^{-2})$	$P(\varepsilon/\sigma^2)$	$U/N(\varepsilon)$	$L(\sigma)$	$\Delta n(\sigma^{-2})$	$D(\sigma^2/\tau)$
1	0.70	0.34	0.155	−1.08	27.44	0.09	0.076
2	0.60	0.34	0.098	−1.19	27.44	0.11	0.067
3	0.50	0.34	0.042	−1.45	27.44	0.16	0.054
4	0.60	0.70	0.524	−2.04	19.12	0.07	0.013

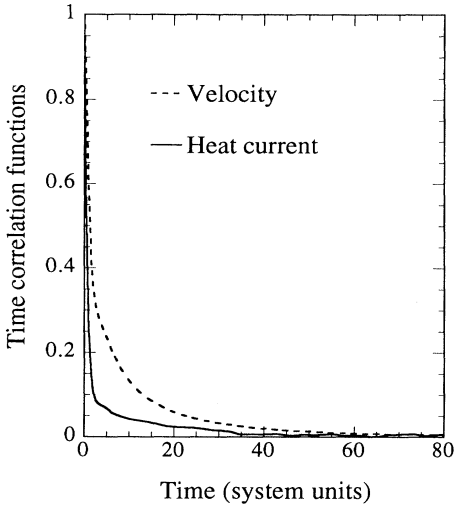

FIG. 2. Normalized time-correlation functions of velocity and heat current for $n=0.34$ and $T=0.6$ (state 2).

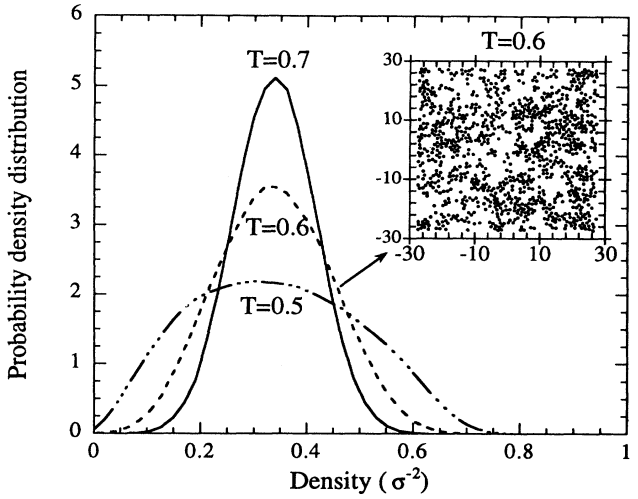

FIG. 3. Density probability distribution for the three supercritical states. The inset is a snapshot showing the instantaneous positions of the particles in state 2 ($n=0.34$ and $T=0.6$); the coordinates of the particles are given in system units (σ).

lar the decay due to the transfer of potential energy at short times and transfer of kinetic energy at long times.

B. Density fluctuations and compressibility

The standard deviation of the density Δn calculated for the three supercritical states increases significantly when the temperature becomes closer to the critical value, thus showing a nearly critical behavior of the density fluctuations. The evolution of the density fluctuation amplitude can be seen more clearly in Fig. 3 where the density probability distribution $P(n)$ is plotted. This distribution has been computed with the block density distribution technique used for the calculation of Δn. $P(n)$ is normalized in such a way that $\int P(n)dn=1$. Here, it is clearly visible that the density tends to have a wider distribution as the critical point is approached. In Fig. 3, we display a snapshot of a large system containing 1024 particles and corresponding to state 2. From the snapshot, one can directly observe the enhanced density fluctuations. Rather than the almost homogeneous distributions expected in the normal liquids or fluids, fully nonhomogeneous distributions of the particles are observed for all the three supercritical states studied in this work.

According to the standard fluctuation theory, the density fluctuation is related to the isothermal compressibility κ_T:

$$\frac{\Delta n}{n}=\left[\frac{nk_BT\kappa_T}{N}\right]^{1/2}. \tag{20}$$

Thus, the increase of the density fluctuation near the critical point indicates also a high compressibility of the fluid. Let us recall, however, that the compressibility obtained from the density fluctuation of the subsystems based on Eq. (20) is not very accurate because of the system-size effects, as discussed in Ref. [14].

C. Thermodynamic parameters

The heat capacity at constant volume, the isothermal compressibility, and $(\partial P/\partial T)_V$ have been computed with Eqs. (2)–(4). The thermal conductivity and the viscosity are calculated by integrating the relevant correlation functions [23]. The resulting values are listed in Table II.

The properties of the supercritical fluids differ significantly from those of the normal fluid; this is noticeable in particular for the heat capacity and the compressibility. While the normal fluid exhibits a liquidlike compressibility, a much higher compressibility is found for the supercritical fluids. Note that the value of κ_T here is many times larger than that for an ideal gas,

TABLE II. MD results: specific heat at constant volume, isothermal compressibility, $(\partial P/\partial T)_V$, thermal conductivity, and viscosity.

State	$c_v k_B$	$nk_BT\kappa_T$	$(k_Bn)^{-1}(\partial P/\partial T)_V$	$\lambda(\varepsilon/\tau T)$	$\eta(\varepsilon\tau/\sigma^2)$
1	1.85	1.84	1.81	0.29	6.2
2	2.75	3.25	1.79	0.35	8.1
3	4.66	12.7	1.65	0.39	12
4	1.55	0.13	4.90	0.71	30

TABLE III. Thermodynamic parameters derived from the MD results listed in Table II.

State	c_p/k_B	γ	$D_T(\sigma^2/\tau)$	$\tau_D(10^3\tau)$	$\Gamma(\sigma^2/\tau)$	$c_s(\sigma/\tau)$	$\tau_s(\sigma/\tau)$
1	7.9	4.26	0.11	6.8	0.37	0.18	152
2	13	4.88	0.08	9.1	0.40	0.14	196
3	39	8.36	0.03	25	0.49	0.08	343
4	4.67	3.01	0.22	1.7	0.67	0.54	35.4

where $nk_BT\kappa_T=1$. On the other hand, the relative importance of the two contributions (potential- and kinetic-energy fluctuations) to the specific heat at constant volume is also varying. While the kinetic part of c_v, which is equal to 1, is more important for the normal fluid, the value of c_v becomes much larger than 1 for the supercritical fluids, thus showing that the potential-energy contribution becomes dominant as the critical point is approached.

The thermodynamic parameters derived from Eqs. (5), (6), and (14)–(16), using the MD results given in Table II are shown in Table III. Here, an increase of c_p and γ, as well as a decrease D_T, are observed as the critical point is approached. All these changes are directly related with the enhanced compressibility, as can be seen from Eqs. (5) and (15). In addition to the strong decrease of the thermal diffusivity, a weak slowing down of the speed of sound is also observed for the near critical states. In comparison with the large variations of c_p and D_T near the critical point, the values of the specific heat and of the thermal diffusivity obtained for the normal fluid state are closer to the standard ones. Note that the values of D_T and Γ for state 4 are rather comparable to the results that can be expected for normal fluids. The values of the acoustic τ_s $(=L/c_s)$ and thermal τ_D $(=L^2/D_T)$ recurrence times, calculated for $N=256$, have also been included in Table III.

D. Hydrodynamic TCF's

The TCF's are calculated mainly for MD systems with $N=256$ particles. To justify the reliability of this system, especially in view of the system-size effects, the MD systems with $N=256$ and 1024 are compared for state 3. The longest density correlation length is observed for this state and the strongest system-size dependence can thus be expected among the states studied here. The TCF's of local density and longitudinal current density obtained from the MD simulations with two system sizes are displayed in Fig. 4. These TCF's are calculated for the smallest k possible for $N=256$. Up to a time comparable with the recurrence time of the smallest system, the results obtained for the two cases exhibit only a slight difference, which is comparable with the statistical error. In the following, we will see that the MD system with $N=256$ is indeed sufficient to produce results accurate enough for the present research purpose.

In Fig. 5, we show the typical k dependence of the density and current TCF's, which are calculated for three different k values. It is clearly visible here that the TCF's decay more slowly for modes with smaller k or longer wavelength, as expected for TCF's of conserved quantities. Since we are more interested in the hydrodynamic limit of the thermal relaxations, we will confine ourselves, in the following discussion, to the TCF's with the smallest possible k.

In Fig. 6, we compare the TCF's for the density, the current, and the temperature obtained by direct MD calculations and from the hydrodynamic theory. The parameters listed in Table III are used to calculate the TCF's with Eqs. (11)–(13). A surprisingly good agreement between the results of MD and the hydrodynamic theory is obtained for all three TCF's. We note that the agreement can still be slightly improved if the TCF's generated with larger MD systems are used, as indicated by Fig. 4. This result confirms the usefulness of the hydrodynamic theory even near the critical point.

The good agreement with the hydrodynamic theory allows us to discuss the TCF's with the help of the analytical solutions given in Sec. II, Eqs. (11)–(13). As can be seen from these equations, the hydrodynamic relaxations of the density and the temperature are governed by two terms corresponding to the thermal diffusion and the acoustic modes, respectively. While the former term is purely exponential, the latter term is a product of the exponential sound attenuation and of the harmonic acoustic oscillation. Furthermore, the relative contributions of these two terms to the TCF's are weighted by the factors

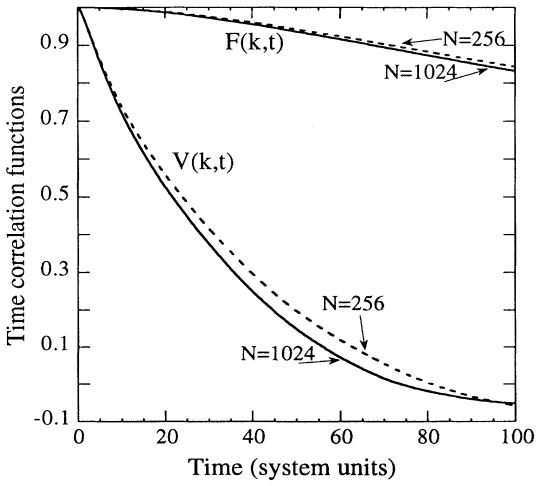

FIG. 4. System-size dependence of the normalized time-correlation functions for local density $F(k,t)$ and longitudinal current $V(k,t)$. The results are plotted for state 3 ($n=0.34$, $T=0.5$) and a value of $k=0.229$.

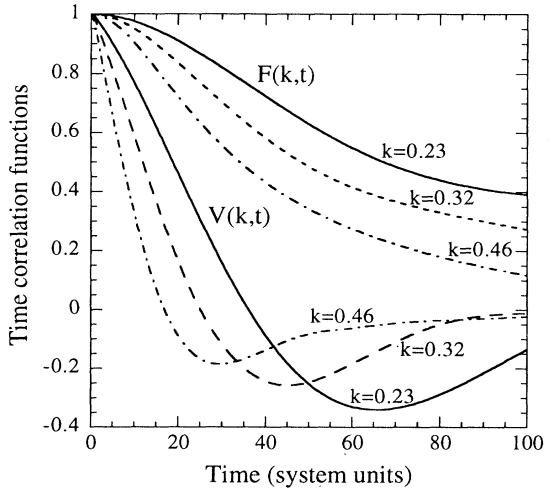

FIG. 5. k dependence of the normalized time-correlation functions for local density $F(k,t)$ and longitudinal current $V(k,t)$. The results calculated for three values of k: $k=2\pi/L,(2\sqrt{2\pi})/L$, $4\pi/L$ are plotted for state 3 ($n=0.34$, $T=0.7$).

containing the ratio of the specific heats γ, which play completely different roles for the density and the temperature TCF's. On the other hand, the TCF of the longitudinal current $V(k,t)$, being the double derivative of $F(k,t)$, is determined mainly by the acoustic mode, as can be seen in Eq. (12). Moreover, $V(k,t)$ becomes identical

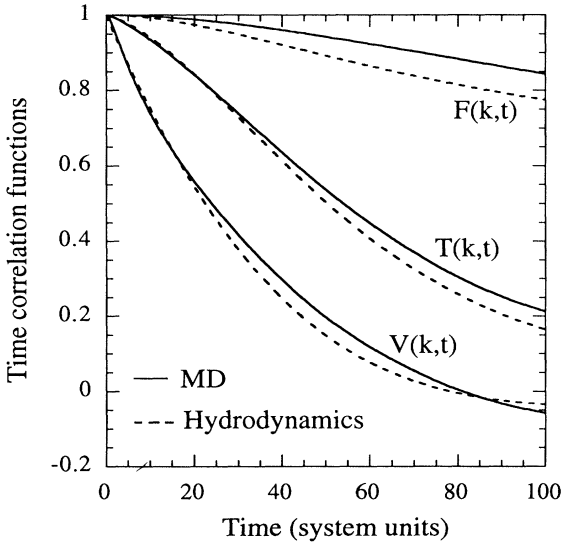

FIG. 6. Comparison of the normalized time-correlation functions for local density $F(k,t)$, longitudinal current $V(k,t)$, and local temperature $T(k,t)$, calculated in two different ways: (i) TCF computed by MD; (ii) TCF calculated with relations (11)–(13) derived from hydrodynamic theory. The results are plotted for state 3 ($n=0.34$, $T=0.5$) with the value of $k=0.229$.

to the acoustic term of $F(k,t)$ and $T(k,t)$ in the hydrodynamic limit ($k\rightarrow 0$).

To compare the thermal relaxations in supercritical and normal fluids, the TCF's of the density, longitudinal current density, and local temperature of states 4 and 2 are shown in Figs. 7(a) and 7(b), respectively. Here, the second, instead of the usual first smallest k, is taken for state 2, to allow for a direct comparison of the TCF's with similar k. Similarly to the VAC computation discussed earlier, all the TCF's in Fig. 7 are calculated in a time range $t=100\tau$ for state 2 and $t=25\tau$ for state 4. Since the correlation time studied is not far from the acoustic recurrence time L/c_s (see Table III), the TCF's at longer times are not explored in the present MD study.

The effects of the acoustic mode are well displayed in the graph of $V(k,t)$. First, the difference of the speed of sound for the two fluid states is clearly exhibited by the different time scales in Figs. 7(a) and 7(b). In fact, the time $t_{\min}$, where $V(k,t)$ has its minimum, is related to the speed of sound by $t_{\min}\cong\pi/kc_s$ in the small k limit, according to Eq. (12). The speeds of sound thus estimated from the MD curves of $V(k,t)$ in Figs. 4–7 really appear to be in accordance with the results based on thermal fluctuations (see Table III). Second, due to the large sound attenuation related to the small value of the speed of sound, the amplitude of the acoustic oscillation in the $V(k,t)$ curve is strongly reduced in the supercritical fluid.

While the TCF's of the current already reach the zero point and the minimum within half of the time span studied, the TCF's of the density decay only to about 50% in Figs. 7(a) and 7(b). The slow decay of $F(k,t)$ relative to $V(k,t)$ is clearly due to the additional thermal diffusion term, according to Eqs. (11) and (12). Although the density TCF's have both a slow decay, a difference can still be observed between the decay rates of the normal and the supercritical states. The slightly oscillatory relaxation of $F(k,t)$ for state 4 apparently comes from the acoustic contribution, whose typical time scale is comparable with that of the thermal diffusion, as is usually the case for normal fluids. However, the rather monotonous decay of the density relaxation in Fig. 7(b) indicates the domination of the thermal diffusion for the supercritical fluid. Furthermore, the acoustic contribution is reduced not only by the long-lived thermal diffusion, but also by the increase of γ, as predicted by Eq. (11).

A difference is also observed between the behaviors of the temperature TCF's for the normal and supercritical fluids. As shown in Fig. 7(a), a rather strong, oscillatory correlation for the temperature TCF remains even after the first minimum for state 4. This indicates that comparable contributions from the thermal diffusion and sound modes are given to the temperature correlation in normal fluids, just as it is in the case for $F(k,t)$ discussed earlier. On the other hand, $T(k,t)$ for the supercritical fluid decays to less than 10% within the much faster acoustic time scale. The absence of the thermal-diffusion-related critical slowing down in the temperature relaxation in Fig. 7(b) is obviously caused by the small value of the prefactor $1/\gamma$ for the diffusion term in Eq. (13). Furthermore, the acoustic oscillation typical for the TCF's in normal fluids is also much reduced here for $T(k,t)$.

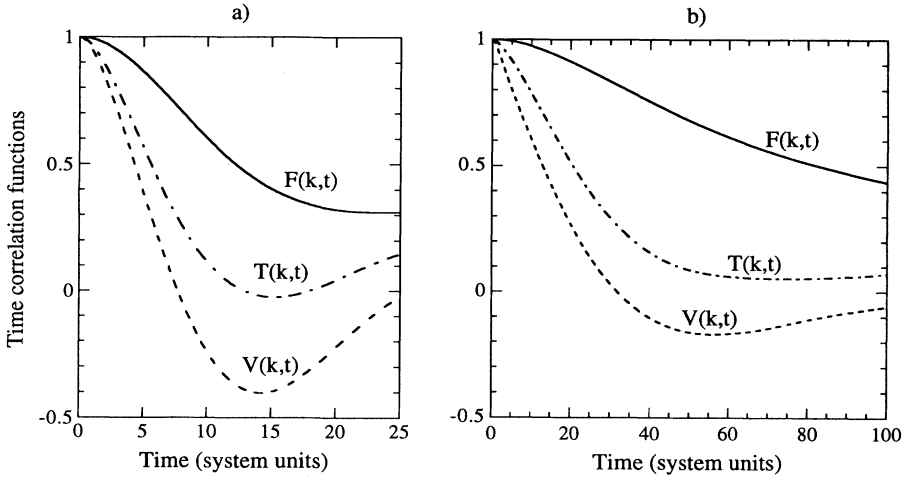

FIG. 7. (a) Normalized time-correlation functions $F(k,t)$, $V(k,t)$, and $T(k,t)$ computed by MD at the same temperature $T=0.6$ for two different densities with the same k value equal to 0.32: (a) normal fluid, $n=0.7$ (state 4), (b) supercritical fluid, $n=0.34$ (state 2).

IV. CONCLUSIONS

Let us sum up the main points that come out of this study. First of all, the fluid that we have simulated seems to be well described by the hydrodynamic equations. This might seem to be a trivial statement since hydrodynamics has been successfully used to model the equilibrium fluctuations in liquids for wavelengths larger than the molecular diameter. However, this conclusion is not really obvious since it implies that the correlation length, which appears near the critical point, is comparable to, although always smaller than the system size. We are able to draw this conclusion from the comparison made between the time dependence of the MD-computed density-density, current-current, and temperature-temperature correlation functions, on the one hand, and the Landau-Placzek form of these same time-correlation functions on the other hand. We stress that the last expressions [see Eqs. (11)–(13)] are computed with thermodynamic parameter values that are independently calculated.

The second point we would like to underline is the following: the values of the thermodynamic parameters that characterize the static and dynamic fluid behavior are, for the studied supercritical states, anticipating the critical point. As can be seen from the tables in the text, the specific heat at constant pressure and the compressibility have large values compared to what is usually computed in a liquid, for example. This increase becomes very important as we approach the critical region. As a consequence, the thermal diffusivity has a low value, giving rise to a quite measurable slowing down for the relaxation of the entropy mode. The effect is less pronounced for the speed of sound, which decreases and becomes barely noticeable for the sound adsorption coefficient, which remains nearly unchanged. This is consistent with what can be expected as general fluid behavior from experimental results.

Since divergences can only be expected in the thermodynamic limit, it is extremely difficult to predict the effects linked to criticality in systems made of a few hundred particles. All the results that we have obtained seem consistent with the following interpretation: the models of a few hundred particles are able, in the supercritical region, to display an unusual behavior that is understood as that of a highly compressible fluid. On the scales we investigated. Navier-Stokes hydrodynamics is still a valid description. In some sense, our results extend the studies made by Rovere, Heermann, and Binder [14] to the dynamic properties. As they did, we have been obliged to work with two-dimensional systems to reduce the computational cost of the simulations.

An important motivation for the present work is the characterization of fluid behavior near criticality. In this respect, let us stress the very unusual behavior of the temperature-temperature TCF in the supercritical region. Most of the temperature relaxation in Fig. 7(b) is driven by the isoentropic acoustic mode, as can be seen from the comparison with the current-current TCF, which is purely acoustic, and with the density-density TCF, which is mostly isobaric and (slowed-down) diffusive. This is in contrast with the usual liquidlike behavior where the temperature is diffusive, whereas the density is driven by sound waves. One should stress that the so-called "normal" state that we have studied for comparison does not display a very different behavior from the critical one; this can be understood since its temperature is still supercritical and some of the thermodynamic parameters will show unusual values (γ, for example, is around 3). Had we chosen a liquid state near the triple point, the difference would have been more striking, but the comparison also would have been more difficult to establish.

This last point is important in the perspective of using nonequilibrium MD in order to simulate directly the transport processes in highly compressible fluids. The present study, in this respect, produces evidence of the ability of the MD technique to reproduce the physical mechanisms taking place near the critical point in the region where the hydrodynamic description is still valid. Work in the direction of a direct modeling is in progress and will be reported in the future.

ACKNOWLEDGMENTS

We want to acknowledge fruitful discussions with Daniel Beysens of CEA-Saclay. This work has been financially supported by the Centre National d'Etudes Spatiales through Contract No. 92/CNES/0418. Financial support of the Belgian Government Services de Programmation de la Politique Scientifique (Contract No. IT/SC/27) is also acknowledged.

[1] A. Onuki, H. Hao, and R. A. Ferrell, Phys. Rev. A **41**, 2256 (1990); A. Onuki and R. A. Ferrell, Physica A **164**, 245 (1990).
[2] B. Zappoli, D. Baily, Y. Garrabos, B. Le Neindre, P. Guenoun, and D. Beysens, Phys. Rev. A **41**, 2264 (1990).
[3] B. Zappoli, Phys. Fluids **4**, 1040 (1992).
[4] P. Guenoun, B. Khalil, D. Beysens, Y. Garrabos, F. Kammoun, B. Le Neindre, and B. Zappoli, Phys. Rev. E **47**, 1531 (1993).
[5] K. Nitsche and J. Straub, in *Proceeding of the Sixth European Symposium on Material Sciences Under Microgravity Conditions, Bordeaux, France, 1986,* edited by European Space Agency (Paris, 1987), Vol. SP-256, p. 109.
[6] J. Straub and K. Nitsche, Fluid Phase Equilib. **88**, 183 (1993).
[7] *Phase Transitions and Critical Phenomena,* edited by C. Domb and M. S. Green (Academic, London, 1976), Vols. 5A and 5B.
[8] L. Landau and E. Lifshitz, *Fluid Mechanics* (Pergamon, London, 1963).
[9] H. E. Stanley, *Introduction to Phase Transitions and Critical Phenomena* (Clarendon, Oxford, 1971).
[10] M. P. Allen and D. J. Tildesley, *Computer Simulation of Liquids* (Clarendon, Oxford, 1987).
[11] W. A. Alley and B. J. Alder, Phys. Rev. A **27**, 3158 (1983); M. Schoen and C. Hoheisel, Mol. Phys. **57**, 445 (1986).
[12] A. Z. Panagiotopoulos, Mol. Phys. **61**, 813 (1987).
[13] B. Smit, Ph.D. thesis, University of Utrecht, 1990; B. Smit, in *Computer Simulation in Chemical Physics,* edited by M. P. Allen and D. J. Tildesley (Kluwer Academic, Dordrecht, 1992).
[14] M. Rovere, D. W. Heermann, and K. Binder, J. Phys. Condens. Matter **2**, 7009 (1990).
[15] L. J. Chen, M. Robert, and K. P. Shukla, J. Chem. Phys. **93**, 8254 (1990); K. P. Shukla and M. Robert, Mol. Simulation **8**, 133 (1991).
[16] F. F. Abraham, Phys. Rep. **53**, 93 (1979).
[17] J. P. Hansen and I. R. McDonald, *Theory of Simple Liquids* (Academic, New York, 1986).
[18] W. G. Hoover, *Computational Statitical Mechanics* (Elsevier, Amsterdam, 1991); see also S. Nosé, in *Computer Simulations in Materials Science,* edited by M. Meyer and V. Pontikis (Kluwer Academic, Dordrecht, 1991).
[19] J. L. Lebowitz, G. K. Percus, and L. Verlet, Phys. Rev. **153**, 250 (1967).
[20] M. H. Ernst, Physica **32**, 252 (1966); P. Résibois, *ibid.* **59**, 587 (1972).
[21] L. P. Kadanoff and P. C. Martin, Ann. Phys. **24**, 419 (1963).
[22] See Ref. [16], p. 283.
[23] See Ref. [10], p. 60.